ORIGINAL PAPER

Effects of iron limitation on carbon balance and photophysiology of the Antarctic diatom *Chaetoceros* cf. *simplex*

Deborah Bozzato[1,2] · Torsten Jakob[1] · Christian Wilhelm[3] · Scarlett Trimborn[4,5]

Abstract

In the Southern Ocean (SO), iron (Fe) limitation strongly inhibits phytoplankton growth and generally decreases their primary productivity. Diatoms are a key component in the carbon (C) cycle, by taking up large amounts of anthropogenic CO_2 through the biological carbon pump. In this study, we investigated the effects of Fe availability (no Fe and 4 nM $FeCl_3$ addition) on the physiology of *Chaetoceros* cf. *simplex*, an ecologically relevant SO diatom. Our results are the first combining oxygen evolution and uptake rates with particulate organic carbon (POC) build up, pigments, photophysiological parameters and intracellular trace metal (TM) quotas in an Fe-deficient Antarctic diatom. Decreases in both oxygen evolution (through photosynthesis, P) and uptake (respiration, R) coincided with a lowered growth rate of Fe-deficient cells. In addition, cells displayed reduced electron transport rates (ETR) and chlorophyll a (Chla) content, resulting in reduced cellular POC formation. Interestingly, no differences were observed in non-photochemical quenching (NPQ) or in the ratio of gross photosynthesis to respiration (GP:R). Furthermore, TM quotas were measured, which represent an important and rarely quantified parameter in previous studies. Cellular quotas of manganese, zinc, cobalt and copper remained unchanged while Fe quotas of Fe-deficient cells were reduced by 60% compared with High Fe cells. Based on our data, Fe-deficient *Chaetoceros* cf. *simplex* cells were able to efficiently acclimate to low Fe conditions, reducing their intracellular Fe concentrations, the number of functional reaction centers of photosystem II (RCII) and photosynthetic rates, thus avoiding light absorption rather than dissipating the energy through NPQ. Our results demonstrate how *Chaetoceros* cf. *simplex* can adapt their physiology to lowered assimilatory metabolism by decreasing respiratory losses.

Keywords Southern Ocean · Phytoplankton · Trace metals · Primary production · Respiration

✉ Deborah Bozzato
d.bozzato@rug.nl

[1] Institute of Biology, Plant Physiology, University of Leipzig, Leipzig, Germany

[2] Groningen Institute for Evolutionary Life Sciences, University of Groningen, Groningen, The Netherlands

[3] Saxon Institute of Biotechnology, Leipzig, Germany

[4] Biogeosciences Section, EcoTrace, Alfred Wegener Institute, Helmholtz Centre for Polar and Marine Research, Bremerhaven, Germany

[5] Marine Botany Department, Faculty 2 Biology/Chemistry, University of Bremen, Bremen, Germany

Introduction

The Southern Ocean (SO) is the world´s largest high nutrients, low chlorophyll (HNLC) region. In this region, despite the abundant supply of macronutrients such as N and P, phytoplankton growth and primary production are mainly limited by the trace element iron (Fe). Numerous studies have revealed the important role of Fe in phytoplankton growth (Boyd et al. 2007; Smetacek et al. 2012), since Fe is required as an important co-factor in enzymes involved in photosynthesis, respiration and nitrogen fixation. Since 1990, numerous laboratory Fe enrichment experiments have been performed, both with Antarctic natural phytoplankton communities (e.g. Feng et al. 2010; Hoppe et al. 2013; Trimborn et al. 2015, 2017) and single phytoplankton species (e.g. van Oijen et al. 2004; van de Poll et al. 2011; Petrou et al. 2014; Trimborn et al. 2019) to unravel the physiological effects of Fe limitation. Fe limitation usually decreases

Photosystem II (PSII) efficiency (Fv/Fm), relative electron transport rate (rETR) and net primary production (NPP) (Hoppe et al. 2013; Zhu et al. 2016; Yoon et al. 2018). Moreover, Fe limitation also controls the photoacclimation status by lowering pigment quotas like chlorophyll a (Chla) and fucoxanthin (van Oijen et al. 2004; Pankowski and McMinn 2009; Feng et al. 2010). Besides these general physiological adjustments, the acclimation to Fe limitation enhances taxon-specific photophysiological differences, for example between haptophytes and diatoms. These different photophysiological acclimation strategies of the two taxa were attributed to the habitats they occupy: diatoms usually thrive in waters with a shallow mixed layer depth, thereby experiencing higher irradiance levels, whereas haptophytes like *Phaeocystis antarctica* are better adapted to low irradiance levels found in a deeply mixed water column (Arrigo and van Dijken 2003).

It is estimated that diatoms contribute to about 40% of marine primary production (Sarthou et al. 2005; Tréguer et al. 2018), playing a key role in the ocean carbon (C) cycle, particularly in the SO. Indeed, the SO is an important net sink for atmospheric CO_2 (Gruber et al. 2019). Many studies have tried to estimate the contribution of phytoplankton to carbon sequestration by quantifying NPP using models, satellite remote sensing data or measured ^{14}C uptake rates (Arrigo et al. 2008; Takao et al. 2012; Hoppe et al. 2018). Nevertheless, a lack of knowledge remains about an important parameter, namely the respiratory losses of organic C by phytoplankton. In order to improve NPP estimates of a given ecosystem, not only should photosynthetic C fixation be considered, but also respiratory C losses by phytoplankton. Due to the differences in day length, light availability and seasonal changes in salinity, the contribution of respiration to the total carbon balance is highly dynamic (Verity 1982; Serret et al. 2015). Although considerable effort has been expended on understanding photosynthesis in aquatic systems, the measurement of phytoplankton respiratory losses has received less attention, primarily due to methodological limitations. While numerous datasets of ^{14}C uptake measurements are available for SO phytoplankton (e.g. Tortell et al. 2008; Kropuenske et al. 2009; Trimborn et al. 2015), only few studies have investigated the respiratory losses together with the assimilation of C (e.g. Tilzer and Dubinsky 1987; Gleitz and Thomas 1992; Thomas et al. 1992; Regaudie-de-Gioux and Duarte 2012; Trimborn et al. 2014). Information on C fixation or respiration rates exists, but rarely have both been measured during the same experiment. The following two studies are emblematic of this issue. In the first study, C uptake measurements were coupled with photophysiological and respiration measurements, however POC production rates were not determined (Trimborn et al. 2014). In the second study, ^{14}C uptake measurements were combined with photophysiological responses and POC build up, but in this

case information about respiration was missing (Petrou et al. 2014). Estimates on respiration rates remain rare yet, as a consequence, respiration data commonly used in models are rough estimates or assumptions (Laws and Bannister 1980; Geider et al. 1998). Thus, respiration in the World's oceans remains a large unknown factor of the global C budget (Marra 2009; Moisan and Mitchell 2018).

Among the plethora of phytoplankton species inhabiting the SO, we have chosen a representative of the genus *Chaetoceros*, which is an important diatom in the SO. In the present study, the effect of low Fe availability on photosynthesis rates (O_2 evolution and POC build up), respiratory losses (O_2 uptake rates), intracellular TM quotas of Fe, zinc (Zn), manganese (Mn), cobalt (Co) and copper (Cu) and the photoacclimation status (pigments, photophysiological parameters) were determined in an Antarctic strain of *Chaetoceros* cf. *simplex*. To our knowledge, no laboratory experiments have explicitly investigated all these processes together in an Antarctic diatom under Fe limitation.

Materials and methods

Experimental conditions

The Antarctic diatom *Chaetoceros* cf. *simplex* used in this study was isolated in 1999 by Thomas Mock (obtained from Dr. Steffi Gäbler-Schwarz, AWI Bremerhaven, Germany). This culture is not axenic, but unialgal and frequently diluted with fresh culture medium. Using inverted light microscopy, no bacteria were observed in the stock culture or during the experiment. The culture was kept for more than 6 months in stock cultures with Fe-deplete and -replete natural Antarctic seawater medium. For the preacclimation phase (over 2 weeks) and the main experiment, the diatom was grown at 2 °C in semi-continuous dilute cultures at an irradiance (E) equal to 100 µmol photons m^{-2} s^{-1} with a 16:8 h light:dark cycle, using light-emitting diodes (LED) lamps (SolarStinger LED SunStrip Marine Daylight, Econlux). Irradiance measurements were integrated in the visible part of the electromagnetic spectrum (400–700 nm), i.e. Photosynthetically Active Radiation (PAR), henceforth referred to as E_{PAR}, using a 4p-sensor (Walz, Effeltrich, Germany) connected to a LI-1400 datalogger (Li-Cor, Lincoln, NE, United States). The F 2_R^{-1} medium (Guillard and Ryther 1962) was prepared from sterile-filtered (0.2 µm) natural low-Fe (0.12 nmol L^{-1}) Antarctic seawater (sampled during the Antarctic Circumpolar Expedition, January 1st, 2017, 59° 61′ S 148° 64′ W), supplemented with chelexed (ChelexR 100, Sigma-Aldrich, Merck) macronutrients (100 µmol L^{-1} Si, 100 µmol L^{-1} NO_3, 6.25 µmol L^{-1} PO_4) and vitamins (30 nmol L^{-1} B_1, 23 nmol L^{-1} B_7, and 0.228 nmol L^{-1} B_{12}). Two different trace metal mix were added to this seawater:

either (i) a trace metal mix containing no Fe (Low Fe treatment) or (ii) an addition of 4 nM $FeCl_3$ (High Fe treatment). The trace metal mixture contained zinc (0.16 nmol L^{-1}), copper (0.08 nmol L^{-1}), cobalt (0.09 nmol L^{-1} Co), molybdenum (0.05 nmol L^{-1}), and manganese (1.9 nmol L^{-1}). These trace metal additions were adjusted to maintain the ratio of the original F 2^{-1} recipe and represent trace metal concentrations typical for Antarctic HNLC waters. 4-L polycarbonate incubation bottles (Nalgene, Thermo Fisher Scientific, Waltham, MA USA) were used and triplicates of each treatment were run in parallel. Over the experiment, cells grew in exponential growth phase and were harvested at cell densities of $49,228 \pm 3299$ and $33,496 \pm 1094$ cells mL^{-1} for the Low Fe and High Fe treatment, respectively. Seawater carbonate chemistry remained stable over the whole duration of the experiment (Online Resource 1). The main experiment lasted 8 days for the Low Fe treatment and 7 days for the High Fe treatment.

In order to minimize Fe contamination, all sampling and handling of the incubation bottles were conducted under a laminar flow hood (Class 140 100, Opta, Bensheim, Germany) using trace metal clean techniques. Briefly, all culture bottles were soaked for 1 week in 1% Citranox solution (Sigma-Aldrich, St. Louis, MO, USA) and subsequently for another 1 week in 1 M hydrochloric acid (high-performance liquid chromatography grade, Merck Millipore Corporation). Between each soaking step, the bottles were rinsed seven times with ultrapure water (Merck Millipore Corporation). Finally, the trace metal-cleaned equipment/bottles were air dried under a clean bench (U.S. class 100) and stored in three polyethylene (PE) bags until usage.

Determination of total dissolved iron concentrations and cellular trace metals quotas

All labware used for analysis was pre-cleaned according to the GEOTRACES cookbook (Cutter et al. 2017). To determine the concentration of total dissolved Fe (dFe) in the Antarctic seawater, all culture medium (without cells) and incubation (with cells) bottles of each treatment were sampled at the end of the experiments. To this end, 100 mL of each sample were filtered (HCl-cleaned 0.2-µm polycarbonate filters, 47 mm, Nuclepore, Whatman, GE Healthcare, Chicago, IL, USA) using a trace metal clean filtration system under a laminar flow hood (Class 100, Opta, Bensheim, Germany). The filtrate was then filled into a 125-mL HCl-cleaned PE bottle and stored triple-bagged at 2 °C until analysis. Between each filtration, the filtration system was cleaned in an acid bath with 1 M HCl and rinsed with Milli-Q. Prior to dFe analysis, all 0.2 µm prefiltered seawater samples were acidified to pH 1.7 with sub-boiled HNO_3 (distilled 65% HNO_3, pro analysis,

Merck) and irradiated for 1.5 h using a UV power supply system (7830) and photochemical lamp (7825) from ArcGlass to provide total dissolved concentrations of Cu and Co (Biller and Bruland 2012). Mn, Fe, Co, Cu and Zn concentrations in seawater samples were analyzed via external calibration using a SeaFAST system (Elemental Scientific) coupled to an Element2 (Thermo Scientific) mass spectrometer. Standards for external calibration were prepared from natural iron-poor seawater spiked with commercially available ICP-MS single element standards (SCP Science; 1000 mg L^{-1}). This procedure reduced possible interference by the matrix and enabled analysis of low concentrations of the elements of interest. To assess the accuracy and precision of the method, a NASS-7 (National Research Council of Canada) reference standard was also analyzed in a 1:10 dilution (corresponding to environmentally representative concentrations) at the beginning and end of a batch run ($n = 5$). Recoveries for Fe were equal to 2.00 ± 0.02 mg g^{-1}, with no significant differences between the measured and certified values of the NASS-7 (i.e., 1.85 ± 0.19 mg g^{-1}).

To determine intracellular TM (Fe, Zn, Mn, Co and Cu) contents, phytoplankton cells were collected onto 0.2-µm acid-cleaned PC filters (EMD Millipore, Darmstadt, Germany), and rinsed for 15 min with a 0.1 M oxalic acid wash to remove trace metals bound to the cell surface (Hassler and Schoemann 2009). Finally, the filters were rinsed with filtered seawater and placed into TM-cleaned 30-mL polytetrafluoroethylene (PTFE) vials. Intracellular TM contents were subsequently analyzed via ICP-MS following a digestion with HNO_3 and HF (Ho et al. 2003; Twining and Baines 2013) in a pressure digestion system (PicoTrace, DAS 30). All filters were digested for 16 h at 180 °C using 5 mL of sub-boiled HNO_3 (distilled 65%, p.a., Merck) and 0.5 mL of HF (ROTIPURAN® Ultra 48%, Carl Roth) followed by the addition of 1 mL of Milli-Q water. The volume of the cell extract was then evaporated on a 140 °C hot plate and the evaporated was passed through a NaOH solution, which effectively neutralized it. 0.2 mL of sub-boiled HNO_3 (distilled 65%, p.a., Merck) and 0.8 mL of Milli-Q water were then added and the solution was heated to 50 °C for 4 h to resuspend the cell extract before it was transferred into 10-mL TM cleaned polypropylene (PP) vials. Lastly, 10 µL of Rh (1 mg L^{-1}) was added as internal standard and the volume was brought up to 10 mL using Milli-Q water, before subsequent analysis on a high resolution ICP-MS (Element2, Thermo Scientific). Acid (5 mL of sub-boiled HNO_3, 0.5 mL HF) and two filter blanks as well as the BCR-414 (Plankton reference material, Sigma Aldrich, St. Louis, MO, United States) samples were also processed and analyzed in order to assure low background TM values as well as digestion quality. Intracellular TM contents were then normalized per cell or POC.

Fluorescence measurements

Chlorophyll a (Chla) fluorescence was measured with a fast repetition rate fluorometer (FRRf, FastOcean PTX sensor, Chelsea Technologies Group Ltd, West Molesey, UK) connected with a FastAct Laboratory system (Chelsea Technologies Group Ltd). All measurements were performed at 2 °C after a 10 min dark acclimation period. The excitation wavelength of the fluorometer's LED was 450 nm, with an automated adjustment of the E_{PAR} to 1.2×10^{22} µmol photons $m^{-2} s^{-1}$. A single turnover mode was set with a saturation phase consisting of 100 flashlets on a 2 µs pitch followed by a relaxing phase of 40 flashlets on a 50 µs pitch. According to Kolber et al. (1998), photosynthetic efficiency was determined by measuring the minimum (Fo) and maximum fluorescence (Fm) to calculate the maximum quantum yield of photochemistry in PSII (Fv/Fm) using the following equation:

$$Fv/Fm = (Fm - Fo)/Fm \tag{1}$$

For the measurement of photosynthesis versus irradiance curves (P–E curves), five actinic light levels (21, 50, 107, 207, 415 µmol photons $m^{-2} s^{-1}$) alternating with dark periods were applied for 5 min each. The effective (see below) and the maximum quantum yields were measured six times at the end of each light and dark period, respectively. The FRRf device supplied actinic irradiance and the irradiance level was previously checked with a light sensor (ULM-500 Universal Light Meter equipped with a Spherical Micro Quantum Sensor US-SQS, Walz GmbH, Effeltrich, Germany). Absolute electron transport rates (aETR, $e^- PSII^{-1} s^{-1}$) at each light level were calculated following Suggett et al. (2004, 2009):

$$aETR = \sigma PSII \cdot ((Fq'/Fm')/(Fv/Fm)) \cdot E \tag{2}$$

where $\sigma PSII$ is the functional absorption cross section of PSII photochemistry ($nm^2 PSII^{-1}$). $Fq' Fm'^{-1}$ denotes the effective PSII quantum yield under ambient light and E represents the respective irradiance level (µmol photons $m^{-2} s^{-1}$). Using the Stern–Volmer equation, non-photochemical quenching (NPQ) of Chla fluorescence was calculated as $(Fm Fm'^{-1}) - 1$ (Bilger and Björkman 1990).

The photosynthesis-irradiance (P–E) curves based on fluorescence measurements were fitted according to Eilers and Peeters (1988). The fitting parameters a, b, and c describe the influence of photoinhibition, the saturation level, and the initial slope of the P–E curve, respectively. Hereby, the term 'photoinhibition' is related to a decrease of photosynthetic activity at PSII due to excessive degradation of the D1 protein particularly at high irradiance (Murata et al. 2007). In the fluorescence measurements, photoinhibition leads to a quenching of Chl a fluorescence indicated by a decrease of

PSII quantum yield and accordingly by a decrease of aETR (Horton et al. 1994). The maximum absolute transport rate ($aETR_{max}$) and the light-saturating index (E_k) were calculated as:

$$aETR_{max} = 1/b + 2\sqrt{a \cdot c} \tag{3}$$

$$E_k = c/b + 2\sqrt{a \cdot c} \tag{4}$$

In addition to the parameters named above, the analysis software of the FRRf FastPro8 (Chelsea Technologies Group Ltd, West Molesey, UK) provides a measure of the connectivity factor of adjacent PSII light harvesting complexes (P, dimensionless), the functional absorption cross section of PSII's photochemistry ($\sigma PSII$, nm^2) and the number of functional PSII reaction centers per volume ($RCII_{vol}$, nmol m^{-3}). The latter parameter was then normalized to cell number to obtain cellular concentrations of RCII ($RCII_{cell}$, amol $cell^{-1}$).

After the completion of the P–E curve, an additional dark-adaptation period of 10 min was applied, followed by a single turnover flashlet to check for recovery of PSII. Using the Fv/Fm measured before and after the P–E-curve, the yield recovery was calculated and given as % of the initial Fv/Fm (before the P–E-curve). All measurements ($n = 3$) were conducted at the growth temperature of 2 °C.

Oxygen-based photosynthesis and respiration rates

Photosynthesis and respiration rates were measured using an oxygen microsensor system (PreSens, Regensburg, Germany). From each experimental condition, cells were harvested by gentle filtration of 400–500 mL culture over a 2-µm membrane filter (Isopore, Millipore) to obtain a volume of about 4–6 mL (equal to a Chla concentration of 2–3 µg mL^{-1}). Subsequently, the concentrated cell suspension was transferred into a special custom-made cuvette where an implantable oxygen microsensor was placed (PreSens) and maintained at 2 °C under continuous gentle stirring. For the measurement of the oxygen-based P–E curves, *Chaetoceros* cf. *simplex* cells were dark-adapted for 10 min and then exposed for 5 min to each of five increasing E_{PAR} (45, 90, 185, 302, 455 µmol photons $m^{-2} s^{-1}$), alternating with a 5 min dark phase between each increasing E_{PAR}. The E_{PAR} was provided by a light projector equipped with neutral density filters. Each E_{PAR} was checked with a light sensor as described above (subsection "Determination of total dissolved iron concentrations and cellular trace metals quotas"). After the measurements, samples were taken for determination of Chla concentration of the cell's concentrate, filtered onto GF/F filters and stored at − 80 °C. Chla was subsequently extracted in 1.6 mL acetone (overnight in darkness, 4 °C)

and determined with a calibrated Turner Designs fluorometer (Model 10–000 R, Mt. View, Canada).

Photosynthetic rates were calculated using the oxygen solubility as a function of the growth medium's salinity and the measuring temperature (Benson and Krause 1984). Gross oxygen production (GP) and net oxygen production (NP) are reported in μmol O_2 (mg Chla)$^{-1}$ h^{-1}. GP was derived by correcting the net oxygen evolution rate for the corresponding dark respiration rate [R; μmol O_2 (mg Chla)$^{-1}$ h^{-1}]. GP_{max} and NP_{max} in the following sections refer to GP and NP values obtained at the maximal E_{PAR} investigated (i.e., 455 μmol photons m^{-2} s^{-1}). The P–E curves based on gross oxygen production were fitted according to Eilers and Peeters (1988).

Growth and cell size determination

Cell samples were fixed with Lugol's solution and stored at 2 °C in the dark until counting. Cell numbers were determined using Utermöhl chambers (Hydrobios, Altenholz, Germany) on an inverted microscope (Zeiss Axiovert 200). After a settling time of at least 24 h, *Chaetoceros* cf. *simplex* cells were counted in stripes in an Utermöhl chamber until at least 400 cells had been counted. A magnification of ×400 in combination with a ×1.6 optovar was used for counting. The cell numbers were plotted on a logarithmic scale and the slope of the linear regression was used to determine growth rates (Fanesi et al. 2016). Cellular biovolume was calculated according to Hillebrand et al. (1999), measuring at least 50 cells for each treatment.

Particulate organic carbon and nitrogen content

For the analyses of particulate organic carbon (POC) and particulate organic nitrogen (PON) content, at the end of the experiment 750 mL of each *Chaetoceros* cf. *simplex* culture flask were filtered onto pre-combusted (500 °C, 15 h) 25-mm GF/F filters (Whatman). One filter blank was taken for each sampled bottle. Samples were stored in combusted glass petri dishes at − 20 °C until sample preparation. Prior to the analysis, filters were dried at 60 °C overnight before they were acidified with 200 μL of 0.2 M HCl to remove the inorganic C. After being dried again at 60 °C overnight, filters were coated in tin foil and compressed into small pellets. Samples were analysed with an automated carbon–nitrogen elemental analyser (Euro EA—CN Elemental Analyzer, HEKAtech GmbH, Wegberg, Germany). POC and PON contents were corrected for blank measurements and normalized to cell density and the filtered volume to yield cellular quotas. Daily POC production rates were calculated by multiplication of the cellular quota with the specific growth rate of the respective treatment. The molar ratio of cellular carbon

to nitrogen (C:N) was calculated by dividing the cellular content of POC (mol) by the cellular content of PON (mol).

Analysis of pigments

For the analysis of pigments, 750 mL of each *Chaetoceros* cf. *simplex* incubation were filtered onto 25-mm glass fiber filters (GF/F, Whatman). The filters were frozen immediately in liquid nitrogen (N_2) and stored at − 80 °C. Before analysis, pigments were extracted from the GF/F filters for 24 h at 4 °C in the dark using 90% acetone (v/v). After centrifugation (5 min, 4 °C, 13000 g) and filtration through a 0.45-μm pore size nylon syringe filter (Nalgene®, Nalge Nunc 241 International, Rochester, NY, USA), total pigment concentrations were determined via reverse HPLC (LaChromElite system, VWR, Darmstadt, Germany). A Spherisorb ODS-2 column (5-μm particle size; Waters, Milford, MA, USA) was used for the separation of the pigments, applying a gradient following Wright et al. (1991). Peaks were detected at 440 nm and identified as well as quantified by co-chromatography with standards (DHI Lab Products, Hørsholm, Denmark) using the software EZChrom Elite ver. 3.1.3. (Agilent Technologies, Santa Clara, CA, USA). More specifically, concentrations of the light harvesting pigments (LHP): chlorophyll a (Chla), chlorophyll c2 (Chl c2), fucoxanthin (Fuco), and the light protective pigments (LPP) diatoxanthin (Dt), diadinoxanthin (Dd) and ß-carotene were determined and normalized to filtered volume and cell numbers to yield cellular quotas.

Statistics

The effect of Fe availability (Low Fe vs. High Fe) on all experimental parameters was statistically analyzed using one-way analyses of variance (ANOVA) with Bonferroni's multiple comparison post-tests. All statistical analyses were performed using the program GraphPad Prism (Version 5.00 for Windows, Graph Pad Software, San Diego California, USA) and the significance testing was done at the $p < 0.05$ level.

Results

Chlorophyll a-based fluorescence parameters

Fe availability strongly influenced the photophysiology of *Chaetoceros* cf. *simplex* (Table 1, Bozzato 2019). The maximum PSII quantum yield of dark-adapted cells (Fv/Fm) was significantly lower ($p < 0.001$) in the Low Fe than in the High Fe treatment. The same trend was also observed for the connectivity between adjacent PSIIs (P), where P in the Low Fe treatment was significantly lower, by 27%, than P in the

Table 1 Chla fluorescence-based photophysiological parameters in *Chaetoceros* cf. *simplex* for low Fe and high Fe conditions

	Low Fe	High Fe
F_v/F_m (rel. unit)	0.38 ± 0.01	$0.50 \pm 0.01^*$
P (rel. unit)	0.32 ± 0.03	$0.44 \pm 0.02^*$
$RCII_{cell}$ (amol cell^{-1})	0.60 ± 0.02	$0.81 \pm 0.05^*$
σ_{PSII} (nm^2)	5.35 ± 0.11	$4.77 \pm 0.06^*$

Values represent mean $\pm$ standard deviation ($n=3$). Significant changes ($p<0.05$, ANOVA) relative to the low Fe condition are denoted by *

Table 2 Photophysiological parameters aETR$_{100}$ (determined at 100 µmol photons m^{-2} s^{-1}), E$_k$ and Fv/Fm recovery (%) were determined in *Chaetoceros* cf. *simplex* grown under low Fe and high Fe conditions

	Low Fe	High Fe
aETR$_{100}$ (e$^-$ PSII^{-1} s^{-1})	136.8 ± 7.2	$183.3 \pm 11.2^*$
E_k (µmol photons m^{-2} s^{-1})	33.8 ± 8.2	$124.2 \pm 30.0^*$
Fv/Fm recovery (%)	46.9 ± 1.5	51.0 ± 1.8

Values represent mean $\pm$ standard deviation ($n=3$). Significant changes ($p<0.01$, ANOVA) relative to the Low Fe condition are denoted by *
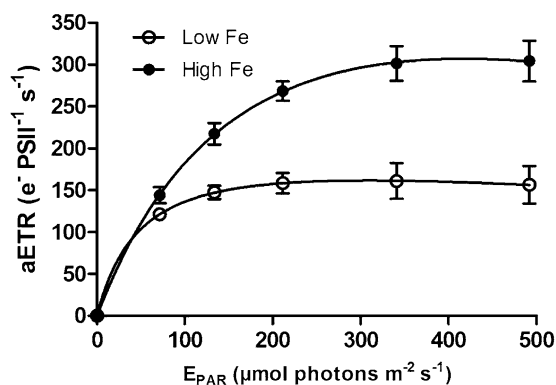
Fig. 1 Absolute electron transport rates (aETRs) in *Chaetoceros* cf. *simplex* grown under Low Fe (open circle) and High Fe (filled circle) conditions. Values represent mean $\pm$ standard deviation ($n=3$)

Fig. 2 Non-photochemical quenching (NPQ) in *Chaetoceros* cf. *simplex* for Low Fe (open circle) and High Fe (filled circle) conditions. Values represent mean $\pm$ standard deviation ($n=3$)

High Fe treatment ($p<0.001$). Similarly, the concentrations of functional reaction centers of PSII per cell ($RCII_{cell}$) were significantly lower, by 26%, in the Low Fe compared to the High Fe ($p<0.001$). In contrast, the functional absorption cross sections of PSII, σ_{PSII}, were 10% higher in the Low Fe than in the High Fe treatment.
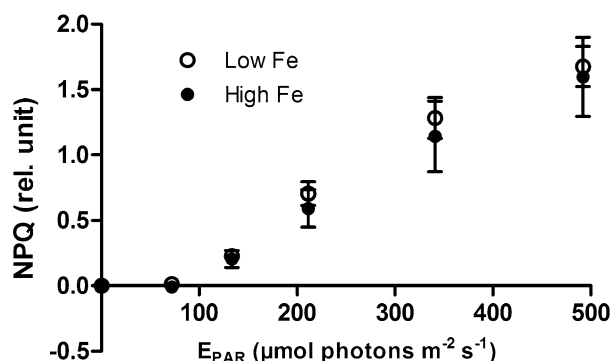
The absolute electron transport rates (aETRs) showed a clear difference between Low Fe and High Fe treatments (Fig. 1). Particularly, the maximum absolute electron transport rates (aETR$_{max}$) of the Low Fe were almost double the High Fe treatment rates, rising from 156 ± 22 to 304 ± 24 e$^-$ PSII^{-1} s^{-1}. aETRs determined at the growth E$_{PAR}$ (aETR$_{100}$) were also significantly lower in the Low Fe compared to the High Fe treatment (Table 2).

The photoacclimation parameter E_k (derived from Chla fluorescence-based P–E curves) revealed a different light acclimation status of *Chaetoceros* cf. *simplex* cells, depending strongly on Fe availability. Accordingly, the E_k value was more than three times greater under High Fe compared to Low Fe availability (Table 2). However, this did not affect the sensitivity to photoinhibition as values of Fv/Fm recovery remained unaltered (Table 2).

Also, the light-induced NPQ of *Chaetoceros* cf. *simplex* cells was not influenced by the different Fe conditions (Fig. 2).

Oxygen-based photosynthesis and respiration rates

Unfortunately, the relatively low Chla concentrations used in the GP and NP measurements caused a low signal/noise ratio and resulted in large standard deviations (Fig. 3, Table 3). Nevertheless, the measured differences between both treatments followed the same trend as aETR measured by Chla fluorescence, i.e. GP and NP of the Low Fe treatment were significantly lower compared to the High Fe treatments. As depicted in Fig. 3a, GP$_{max}$ in the Low Fe treatment was only 24% of the GP$_{max}$ in the High Fe treatment, reaching rates of 95 ± 28 and 399 ± 224 µmol O$_2$ (mg Chla)$^{-1}$ h^{-1} in Low Fe and High Fe conditions, respectively. An even greater difference between Low Fe and High Fe conditions was measured in net photosynthesis (NP) rates (Fig. 3b), with NP$_{max}$ values of 287 ± 224 and 55 ± 28 µmol O$_2$ (mg Chla)$^{-1}$ h^{-1}, respectively. Please note that all values reported in Table 3 were determined at the growth E$_{PAR}$ (i.e., 100 µmol photons m^{-2} s^{-1}).
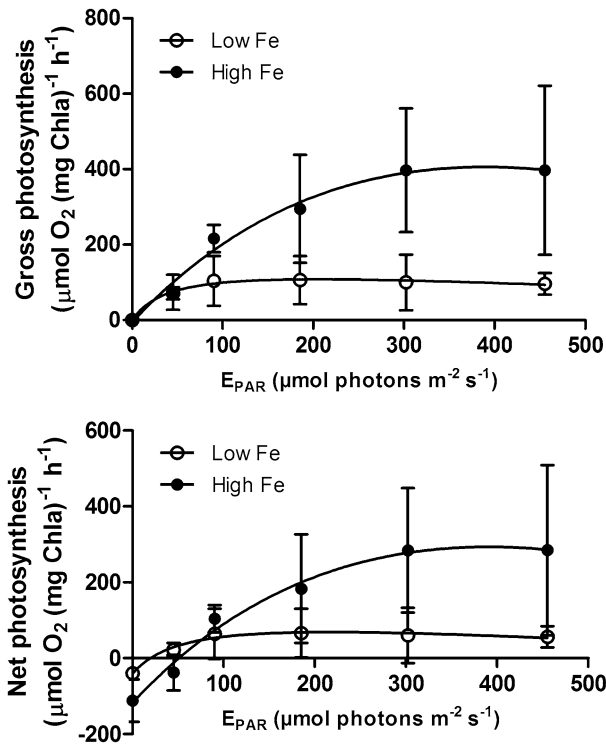
Fig. 3 Gross (**a**) and net (**b**) photosynthesis rates in *Chaetoceros* cf. *simplex* for Low Fe (open circle) and High Fe (filled circle) conditions. Values represent mean ± standard deviation ($n = 3$)

Table 3 Gross and net oxygen production (GP and NP, respectively), respiration (R) and GP:R were determined at 100 μmol photons m^{-2} s^{-1} in *Chaetoceros* cf. *simplex* for Low Fe and High Fe conditions

	Low Fe	High Fe
Gross oxygen production (GP) [μmol O_2 (mg Chla)$^{-1}$ h^{-1}]	99.4 ± 65.5	202.3 ± 36.1
Net oxygen production (NP) [μmol O_2 (mg Chla)$^{-1}$ h^{-1}]	59.6 ± 65.5	89.9 ± 36.1
Respiration (R) [μmol O_2 (mg Chla)$^{-1}$ h^{-1}]	−39.8 ± 8.9	−112.3 ± 56.3*
GP:R	2.9 ± 1.7	2.7 ± 1.6

Values represent mean ± standard deviation ($n = 3$). Significant changes ($p < 0.05$, ANOVA) relative to the Low Fe condition are denoted by *

Similarly, respiration (R) was significantly lower in the Low Fe treatment compared to High Fe ($p < 0.05$, Table 3). Interestingly, the ratio of GP to R (GP:R, Table 3) showed no variations between treatments.

Elemental composition, growth and cell size

The content of particulate organic carbon (POC) and particulate organic nitrogen (PON) per cell varied significantly between the two treatments (Table 4). Cell number normalized POC and PON contents were 18% ($p < 0.01$) and 28% ($p < 0.001$) lower in low Fe than in High Fe treatments, respectively. When the POC values were normalized to cell volume, such differences between the two treatments were not visible anymore (Table 4). With decreasing Fe availability, cell number normalized POC production rates declined (Table 4) while this was not the case when normalized to cell volume. The molar carbon to nitrogen ratios, C:N, were slightly higher in cells grown in the Low Fe than in the High Fe treatment ($p < 0.01$, Table 4).

The growth rates of *Chaetoceros* cf. *simplex* were significantly lower, by 9%, in the Low Fe treatment (0.53 day^{-1}) compared to the High Fe treatment (0.58 day^{-1}) (Table 4). Correspondingly, the cell length/volume was also lower in Fe-deficient compared to Fe-enriched cells.

Pigments

Generally, the pigment content of *Chaetoceros* cf. *simplex* did not differ between both treatments, except for Chla, which was 20% lower in the Low Fe than in the High Fe treatment ($p < 0.01$), and for ß-carotene, which was 43% lower in the Low Fe vs. High Fe treatment ($p < 0.001$; Table 5).

Total dissolved iron concentrations and intracellular trace metals quotas

The concentration of total dFe of the culture medium of the Low Fe and the High Fe treatments were significantly different ($p < 0.0001$), with 0.39 ± 0.02 and 3.07 ± 0.13 nmol

Table 4 Elemental composition, growth rate and cell size of *Chaetoceros* cf. *simplex* for Low Fe and High Fe conditions

	Low Fe	High Fe
POC (pg C cell^{-1})	7.63 ± 0.42	9.26 ± 0.71*
POC$_{vol}$ (pg C μm^{-3})	0.17 ± 0.03	0.16 ± 0.01
Daily POC production rate (pg C cell^{-1} day^{-1})	4.04 ± 0.20	5.39 ± 0.86*
Daily POC$_{vol}$ production rate (pg C μm^{-3} day^{-1})	0.09 ± 0.01	0.09 ± 0.01
PON (pg N cell^{-1})	1.37 ± 0.06	1.76 ± 0.12*
C:N (mol mol^{-1})	6.48 ± 0.10	6.12 ± 0.16*
μ (day^{-1})	0.53 ± 0.02	0.58 ± 0.02*
Cell length (μm)	5.63 ± 0.28	6.44 ± 0.11*
Cell volume (μm^3)	46.37 ± 5.75	58.39 ± 1.80*

simplex for low Fe and high Fe conditions. Values represent mean ± standard deviation ($n = 3$)

Values represent mean ± standard deviation ($n = 3$). Significant changes ($p < 0.05$, ANOVA) relative to the low Fe condition are denoted by *

Table 5 Cellular concentrations (fg cell^{-1}) of the light harvesting pigments (LHP): chlorophyll a (Chla), chlorophyll c_2 (Chl c_2), fucoxanthin (Fuco), as well as of the light protective pigments (LPP): ß-carotene (ß-car), diadinoxanthin (Dd), diatoxanthin (Dt) and the ratio of LHP:LPP for *Chaetoceros* cf. *simplex* grown under Low Fe and High Fe conditions

	Low Fe	High Fe
Chla	126.5 ± 8.8	158.7 ± 16.5*
Chlc$_2$	17.9 ± 1.7	19.9 ± 3.6
Fuco	75.1 ± 6.1	80.5 ± 12.0
ß-car	2.8 ± 0.3	4.9 ± 0.6*
Dd	22.8 ± 1.7	25.5 ± 8.2
Dt	0.4 ± 0.1	0.5 ± 0.3
LHP:LPP	9.5 ± 0.4	10.5 ± 2.7

Values represent mean ± standard deviation ($n = 3$). Significant changes ($p < 0.01$, ANOVA) in pigment concentrations relative to the Low Fe denoted by *

Table 6 Concentrations of total dissolved iron, zinc, manganese, cobalt, and copper (in nM) were determined in all incubation (with *Chaetoceros* cf. *simplex* cells) and culture medium (without cells) bottles of each treatment (Low Fe and High Fe) at the end of the experiments ($n \geq 3$)

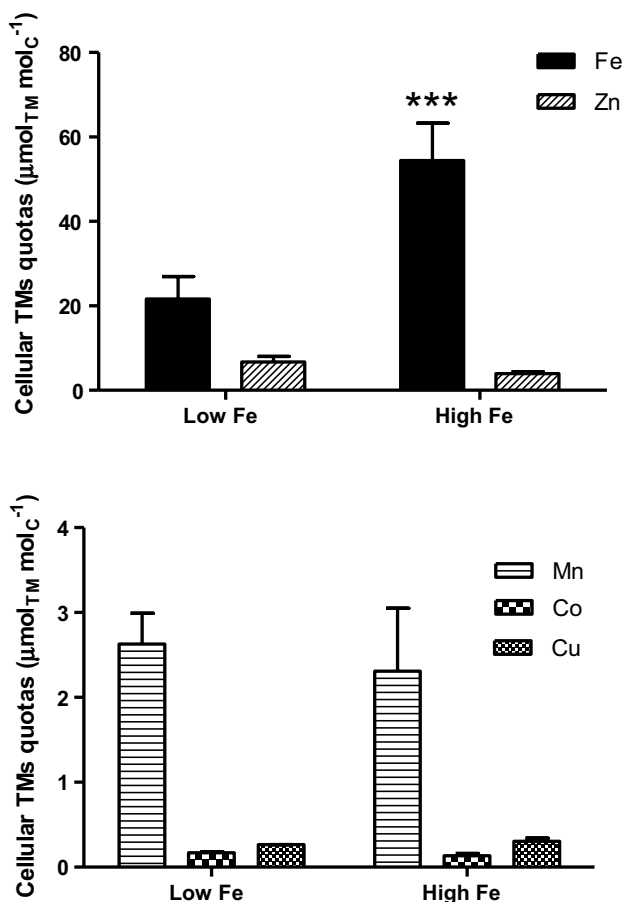|	*Chaetoceros* cf. *simplex*		Culture medium	
	Low Fe	High Fe	Low Fe	High Fe
Fe	0.44 ± 0.15	0.58 ± 0.12	0.39 ± 0.02	3.07 ± 0.13***
Zn	10.79 ± 2.61	9.55 ± 3.23	10.55 ± 0.70	9.37 ± 1.90
Mn	0.56 ± 0.25	0.91 ± 0.34	1.90 ± 0.01	1.82 ± 0.02
Co	0.48 ± 0.01	0.48 ± 0.02	0.43 ± 0.01	0.43 ± 0.02
Cu	0.85 ± 0.05	0.87 ± 0.06	0.96 ± 0.05	0.99 ± 0.05

Significant changes in total dissolved trace metals concentrations of the High Fe relative to the Low Fe are denoted by *** ($p < 0.0001$, ANOVA)

amol cell^{-1}). In contrast, Zn, Mn Co and Cu quotas were not significantly different between the two treatments.

Discussion

Fe is essential for redox-based reactions and is required for photosynthesis, respiration, and the nitrate and sulfur utilization pathways in phytoplankton (Behrenfeld and Milligan 2013; Raven 2013). Measuring both photosynthesis and respiration is essential in order to provide more accurate oceanic primary production rates, a key component of the global carbon cycle, as evident by different model scenarios (e.g. Tilzer and Dubinsky 1987; Lancelot et al. 1991; Arístegui et al. 1996; Quay et al. 2010). Recently it has been shown that the GP:R ratio is a critical parameter to assess the NPP depending on light and temperature conditions (Bozzato et al. 2019). The influence of GP:R ratios on NPP is seasonal-dependent. The present study confirms that also under Fe-limiting conditions the GP:R ratio must be taken into account to assess the real NPP. For the first time, this study presents a novel experimental approach, by combining both photosynthesis and respiration, in order to better understand the effects of Fe-limitation on carbon uptake in the SO. Since Fe is important for the proteins in the electron transport chain (ETC), Fe deficiency directly influences the photosynthetic performance of the cells (Behrenfeld and Milligan 2013). Also in this study, a strong response to Fe depletion was found in different physiological parameters, such as a lower Fv/Fm from 0.50 to 0.38 (Table 1) in the *Chaetoceros* species tested in this work. Similarly, the number of functional reaction centers per cell, RCII$_{cell}$, as well as the connectivity between PSII, P, was lower under Low Fe compared to High Fe, a response commonly observed under Fe limitation (Petrou et al. 2014; Koch et al. 2019; Trimborn et al. 2019). Conversely, the functional absorption

L^{-1}, respectively (Fig. 4). Total dFe concentrations of the High Fe *Chaetoceros* cf. *simplex* incubation bottles were significantly reduced compared to the values of the culture medium High Fe bottles, indicating strong Fe uptake by the High Fe cells over the main experiment. Such uptake was not measured on the Low Fe treatments where no significant differences were found among the other trace metals (Table 6).

The carbon-normalized Fe quotas of *Chaetoceros* cf. *simplex* (expressed as μmol TM:mol C, henceforth referred to as μmol:mol) showed a significant difference between Low Fe and High Fe cells (Fig. 5). The same trend was also observed in the cell-normalized TM quotas (Table 7, expressed as
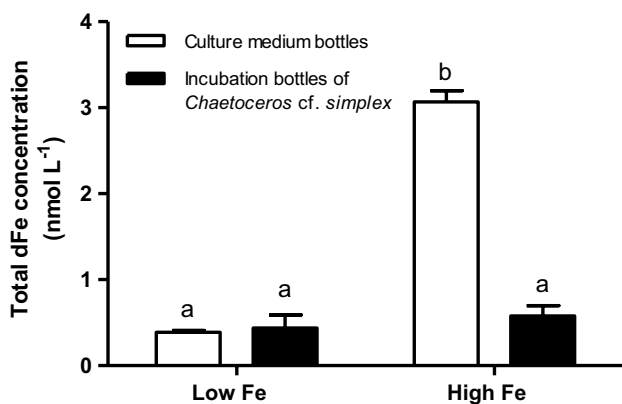
Fig. 4 Concentrations of total dissolved Fe (dFe) determined at the end of the main experiment. Concentrations were measured in the culture medium (white bars) and the incubation bottles of *Chaetoceros* cf. *simplex* cells (black bars), to which either no (Low Fe) or a 4 nM FeCl$_3$ spike was added. Data shown represent mean ± standard deviation ($n \geq 3$). Significant differences (ANOVA) for each parameter are denoted by different letters ($p < 0.0001$)

Fig. 5 Carbon normalized cellular quotas of **a** the trace metals iron (Fe) and zinc (Zn); **b** manganese (Mn), copper (Cu) and cobalt (Co); for *Chaetoceros* cf. *simplex* grown under Low Fe and High Fe conditions. Values represent mean ± standard deviation ($n = 3$). Significant differences for each parameter relative to the Low Fe are denoted by *** ($p < 0.0001$, ANOVA)

Table 7 Cellular contents of Fe, Zn, Mn, Co, and Cu (in amol cell^{-1}) of *Chaetoceros* cf. *simplex* grown under Low Fe and High Fe conditions ($n = 3$, # $n = 2$)

	Low Fe	High Fe
Fe	14.22 ± 3.89#	41.61 ± 4.92***
Zn	4.30 ± 1.01	3.08 ± 0.14#
Mn	1.66 ± 0.18	1.75 ± 0.47
Co	0.11 ± 0.00	0.10 ± 0.01
Cu	0.17 ± 0.01#	0.24 ± 0.04*

Significant changes in intracellular trace metals quotas relative to the Low Fe are denoted by *** or * (respectively, $p < 0.0001$ and $p < 0.05$, ANOVA)

cross sections of PSII, σ_{PSII} was higher in Fe-limited cells. Such a response is attributed to an increase in the ratio of antenna complexes relative to the reaction center core complexes (Greene et al. 1991). It has been suggested that SO

phytoplankton species, in particular, counteract the diminished number of Fe-rich PS reaction centers with a larger σ_{PSII} (Strzepek et al. 2012), as frequently observed for other Antarctic *Chaetoceros* species (Timmermans et al. 2001; van Oijen et al. 2004; Petrou et al. 2014; Trimborn et al. 2019).

Among the different subunits of the photosynthetic apparatus, PSI and cytochrome b_6f have particularly high Fe requirements and represent the limiting components of the electron flow in the thylakoid membranes (Wilhelm and Wild 1984; Strzepek and Harrison 2004). Under Fe limitation, the required Fe cannot be replaced and the cytochrome complexes cannot be substituted by alternative electron carriers. Thus, Fe limitation strongly limited the capacity of aETR both at the growth E_{PAR} (Table 2) and at light saturation (aETR$_{max}$, Fig. 1) in the Low Fe compared to High Fe treatment, which led to a much earlier onset of light saturation, E_k, under Low Fe conditions (Table 2). This is in line with light saturation characteristics previously reported for the Fe limited Antarctic *Chaetoceros simplex* (Petrou et al. 2014). Fe is required in several ETC proteins and the limited Fe availability thus pushed the cell`s physiological machinery to absorb less light. As a consequence of the lowered Fe availability, the *Chaetoceros* cells in the Low Fe treatment exhibited 60% lower intracellular Fe content compared to High Fe cells (Table 7 and Fig. 5). In comparison, there was no difference in the TM quotas of Zn, Mn, Co and Cu between the two treatments.

The response of O_2-based photosynthetic rates (NP and GP, Fig. 3) under Fe deficiency follows the same pattern as for the measured aETRs by Chla fluorescence (Fig. 1). Similarly, NP and GP at growth E_{PAR} were much lower under Fe deficiency (Table 3), with even lower GP$_{max}$ and NP$_{max}$ in the Low Fe compared to High Fe treatment (Fig. 3). The differences in light-saturated GP could be accounted for by a lowered Rubisco content in the Low Fe cells. Indeed, it has already been shown that the relative abundance of the carboxylating enzyme Rubisco decreased in response to Fe starvation (Geider et al. 1993). Furthermore, Wilhelm and Wild (1984) showed that the amount of Rubisco and cytochrome f (cyt f) are regulated in a coordinated manner and therefore the assumed Fe-dependent decrease of cyt b_6f content fits well with the lower GP$_{max}$ under low Fe conditions observed in this study.

To the authors' knowledge, this is the first study combining P and R rates with daily C production of an Fe-limited Antarctic diatom. Indeed, to illustrate the efficiency of the conversion of photosynthetic energy into C biomass production it is worthwhile to compare the photosynthetic rates (aETRs and GP) with the daily C production (Table 4) under Low Fe and High Fe conditions. It becomes evident that the inhibitory effect of Fe limitation was more pronounced for the photosynthetic energy production than for C biomass

production. Moreover, when POC data are normalized to cell volume (POC_{vol}, Table 4) rather than to cell number, an Fe-dependent decrease in POC production is no longer visible (Daily POC_{vol} production rate, Table 4). As has been observed in other diatoms (Timmermans et al. 2001; van de Poll et al. 2009; Alderkamp et al. 2012; Trimborn et al. 2019), *Chaetoceros* cf. *simplex* was able to strongly limit the number of electrons entering the ETC under Fe limitation (Fig. 1). In this way, an overexcitation of the ETC was prevented. This fits with the observed decrease of the light absorption capacity, as indicated by the significantly lower cellular Chla content in Low Fe cells (Table 5). In addition, the lower content of ß-carotene in Low Fe relative to High Fe cells (Table 5) is in line with less functional PSII reaction centers (Tracewell et al. 2001). Lastly, the assumption that a decreased photosynthetic capacity limits the excitation pressure on the ETC is supported by the fact that Fe limited cells were neither forced to increase their extent of NPQ under saturating irradiance (Fig. 2) nor to increase their pool size of light protective pigments (LPP, Table 5). Moreover, the *P–E* curve (Fig. 3) and the Fv/Fm recovery rate (Table 2) did not reveal any indications for an increased sensitivity to high irradiances in cells under Low Fe conditions.

The absence of a difference in NPQ as a result of the different Fe availability is in contrast to the observations for Fe-limited cells of *C. simplex* made by Petrou et al. (2014). However, variations between the experimental setups should be considered. Firstly, the latter species was grown at a lower E_{PAR} of 30 μmol photons m^{-2} s^{-1}, while the E_{PAR} in the present study was much higher (i.e., 100 μmol photons m^{-2} s^{-1}). Secondly, the NPQ_{max} values in Petrou et al. (2014) were obtained at an E_{PAR} 4 times higher than in this study (2260 vs. 492 μmol photons m^{-2} s^{-1}, respectively). Having a closer look at the data from Petrou et al. (2014), the NPQ values in the Fe limited *C. simplex* cells exposed to 500 μmol photons m^{-2} s^{-1} (~ 0.1–0.2) were in a similar range as those of the *Chaetoceros* cf. *simplex* cells from this study.

Besides the simultaneous determination of photosynthesis rates by different methods (variable Chla fluorescence, oxygen evolution, C biomass production), a novel aspect of this study was the measurement of respiration rates in the Antarctic diatom *Chaetoceros* cf. *simplex* (Table 3). The Fe-limited conditions resulted in 65% lower R compared to High Fe conditions at the growth E_{PAR} (Table 3). However, this did not result in any differences in the ratio of photosynthesis to respiration (GP:R, Table 3). This is not a trivial result, since studies investigating the photosynthetic activity of Antarctic phytoplankton are available (e.g. Palmisano et al. 1987; Petrou and Ralph 2011), whereas knowledge about carbon losses due to respiration is very scarce, mainly due to methodological limitations (e.g. Marra 2009; Moisan and Mitchell 2018). Data presented in the literature show

a high variability in the ratio between photosynthesis and respiration (e.g. Vona et al. 2004). Furthermore, the cell size was also lower in the Low Fe vs. High Fe treatment (Table 4), which is a typical response found in Fe-limited cells (e.g. Stefels and van Leeuwe 1998). Thereby, the cells compensate for Fe deficiency and similar POC_{vol} production rates between the two treatments were obtained (Table 4). Overall, these results indicate that the Fe limited cells showed a very efficient acclimation to the lowered assimilatory metabolism by decreasing their respiratory losses. This compensated for the inevitable reduced capacity for photosynthesis under Fe limitation.

Compliance with ethical standards

References

Alderkamp A-C, Kulk G, Buma AGJ, Visser RJW, van Dijken GL, Mills MM, Arrigo KR (2012) The effect of iron limitation on the photophysiolgy of *Phaeocystis antarctica* (Prymnesiophyceae) and *Fragilariopsis Cylindrus* (Bacillariophyceae) under dynamic irradiance. J Phycol 48:45–59. https://doi.org/10.1111/j.1529-8817.2011.01098.x

Arístegui J, Montero MF, Ballesteros S, Basterretxea G, van Lenning K (1996) Planktonic primary production and microbial respiration measured by 14C assimilation and dissolved oxygen changes in coastal waters of the Antarctic Peninsula during austral summer:implications for carbon flux studies. Mar Ecol Prog Ser 132:191–201. https://doi.org/10.3354/meps132191

Arrigo KR, van Dijken GL (2003) Phytoplankton dynamics within 37 Antarctic coastal polynya systems. J Geophys Res 108:425. https://doi.org/10.1029/2002JC001739

Arrigo KR, van Dijken GL, Bushinsky S (2008) Primary production in the Southern Ocean, 1997–2006. J Geophys Res 113:609. https://doi.org/10.1029/2007JC004551

Behrenfeld MJ, Milligan AJ (2013) Photophysiological expressions of iron stress in phytoplankton. Ann Rev Mar Sci 5:217–246. https://doi.org/10.1146/annurev-marine-121211-172356

Benson BB, Krause D (1984) The concentration and isotopic fractionation of oxygen dissolved in freshwater and seawater in equilibrium with the atmosphere1. Limnol Oceanogr 29:620–632. https://doi.org/10.4319/lo.1984.29.3.0620

Bilger W, Björkman O (1990) Role of the xanthophyll cycle in photoprotection elucidated by measurements of light-induced absorbance changes, fluorescence and photosynthesis in leaves of *Hedera canariensis*. Photosynth Res 25:173–185. https://doi.org/10.1007/BF00033159

Biller DV, Bruland KW (2012) Analysis of Mn, Fe Co, Ni, Cu, Zn, Cd, and Pb in seawater using the Nobias-chelate PA1 resin and magnetic sector inductively coupled plasma mass spectrometry (ICP-MS). Mar Chem 130–131:12–20. https://doi.org/10.1016/j.marchem.2011.12.001

Boyd PW, Jickells T, Law CS, Blain S, Boyle EA, Buesseler KO, Coale KH, Cullen JJ, de Baar HJW, Follows M, Harvey M, Lancelot C, Levasseur M, Owens NPJ, Pollard R, Rivkin RB, Sarmiento J, Schoemann V, Smetacek V, Takeda S, Tsuda A, Turner S, Watson AJ (2007) Mesoscale iron enrichment experiments 1993–2005: synthesis and future directions. Science 315:612–617. https://doi.org/10.1126/science.1131669

Bozzato D (2019) The effect of climate change on the carbon balance between photosynthesis and respiration in Antarctic microalgae. Dissertation, University of Leipzig

Bozzato D, Jakob T, Wilhelm C (2019) Effects of temperature and salinity on respiratory losses and the ratio of photosynthesis to respiration in representative Antarctic phytoplankton species. PLoS ONE 14:e0224101. https://doi.org/10.1371/journal.pone.0224101

Cutter G, Casciotti K, Croot P, Geibert W, Heimbürger L-E, Lohan M, Planquette H, van de Flierdt T (2017) Sampling and sample-handlingprotocols for GEOTRACES Cruises. Version 3, August 2017. https://doi.org/10.25607/OBP-2

Eilers P, Peeters J (1988) A model for the relationship between light intensity and the rate of photosynthesis in phytoplankton. Ecol Model 42:199–215. https://doi.org/10.1016/0304-3800(88)90057-9

Fanesi A, Wagner H, Becker A, Wilhelm C (2016) Temperature affects the partitioning of absorbed light energy in freshwater phytoplankton. Freshw Biol 61:1365–1378. https://doi.org/10.1111/fwb.12777

Feng Y, Hare CE, Rose JM, Handy SM, DiTullio GR, Lee PA, Smith WO, Peloquin J, Tozzi S, Sun J, Zhang Y, Dunbar RB, Long MC, Sohst B, Lohan M, Hutchins DA (2010) Interactive effects of iron, irradiance and CO$_2$ on Ross Sea phytoplankton. Deep Sea Res I 57:368–383. https://doi.org/10.1016/j.dsr.2009.10.013

Geider RJ, Roche J, Greene RM, Olaizola M (1993) Response of the photosynthetic apparatus of *Phaeodactylum Tricornutum* (Bacillariophyceae) to nitrate, phosphate, or iron starvation. J Phycol 29:755–766. https://doi.org/10.1111/j.0022-3646.1993.00755.x

Geider RJ, Maclntyre HL, Kana TM (1998) A dynamic regulatory model of phytoplanktonic acclimation to light, nutrients, and temperature. Limnol Oceanogr 43:679–694. https://doi.org/10.4319/lo.1998.43.4.0679

Gleitz M, Thomas DN (1992) Physiological responses of a small Antarctic diatom (*Chaetoceros* sp.) to simulated environmental constraints associated with sea-ice formation. Mar Ecol Prog Ser 88:271–278

Greene RM, Geider RJ, Falkowski PG (1991) Effect of iron limitation on photosynthesis in a marine diatom. Limnol Oceanogr 36:1772–1782. https://doi.org/10.4319/lo.1991.36.8.1772

Gruber N, Landschützer P, Lovenduski NS (2019) The variable Southern Ocean carbon sink. Ann Rev Mar Sci 11:159–186. https://doi.org/10.1146/annurev-marine-121916-063407

Guillard RRL, Ryther JH (1962) Studies of marine planktonic diatoms. I. Cyclotella nana Hustedt, and *Detonula confervacea* (cleve) Gran. Can J Microbiol 8:229–239. https://doi.org/10.1139/m62-029

Hassler CS, Schoemann V (2009) Discriminating between intra- and extracellular metals using chemical extractions: an update on the case of iron. Limnol Oceanogr Methods 7:479–489. https://doi.org/10.4319/lom.2009.7.479

Hillebrand H, Dürselen C-D, Kirschtel D, Pollingher U, Zohary T (1999) Biovolume calculation for pelagic and benthic microalgae. J Phycol 35:403–424. https://doi.org/10.1046/j.1529-8817.1999.3520403.x

Ho T-Y, Quigg A, Finkel ZV, Milligan AJ, Wyman K, Falkowski PG, Morel FMM (2003) The elemental composition of some marine phytoplankton. J Phycol 39:1145–1159. https://doi.org/10.1111/j.0022-3646.2003.03-090.x

Hoppe CJM, Hassler CS, Payne CD, Tortell PD, Rost B, Trimborn S (2013) Iron limitation modulates ocean acidification effects on southern ocean phytoplankton communities. PLoS ONE 8:e79890. https://doi.org/10.1371/journal.pone.0079890

Hoppe CJM, Schuback N, Semeniuk D, Giesbrecht K, Mol J, Thomas H, Maldonado MT, Rost B, Varela DE, Tortell PD (2018) Resistance of Arctic phytoplankton to ocean acidification and enhanced irradiance. Polar Biol 41:399–413. https://doi.org/10.1007/s00300-017-2186-0

Horton P, Ruban AV, Walters RG (1994) Regulation of light harvesting in green plants (indication by nonphotochemical quenching of chlorophyll fluorescence). Plant Physiol 106:415–420. https://doi.org/10.1146/annurev.arplant.47.1.655

Koch F, Beszteri S, Harms L, Trimborn S (2019) The impacts of iron limitation and ocean acidification on the cellular stoichiometry, photophysiology, and transcriptome of *Phaeocystis antarctica*. Limnol Oceanogr 64:357–375. https://doi.org/10.1002/lno.11045

Kolber ZS, Prášil O, Falkowski PG (1998) Measurements of variable chlorophyll fluorescence using fast repetition rate techniques: defining methodology and experimental protocols. Biochim Biophy Acta (BBA) 1367:88–106. https://doi.org/10.1016/S0005-2728(98)00135-2

Kropuenske LR, Mills MM, van Dijken GL, Bailey S, Robinson DH, Welschmeyer NA, Arrigoa KR (2009) Photophysiology in two major Southern Ocean phytoplankton taxa: Photoprotection in *Phaeocystis antarctica* and *Fragilariopsis cylindrus*. Limnol Oceanogr 54:1176–1196. https://doi.org/10.4319/lo.2009.54.4.1176

Lancelot C, Billen G, Veth C, Becquevort S, Mathot S (1991) Modelling carbon cycling through phytoplankton and microbes in the Scotia—Weddell Sea area during sea ice retreat. Mar Chem 35:305–324. https://doi.org/10.1016/S0304-4203(09)90024-X

Laws EA, Bannister TT (1980) Nutrient- and light-limited growth of *Thalassiosira fluviatilis* in continuous culture, with implications for phytoplankton growth in the ocean. Limnol Oceanogr 25:457–473. https://doi.org/10.4319/lo.1980.25.3.0457

Marra J (2009) Net and gross productivity: weighing in with [14]C. Aquat Microb Ecol 56:123–131. https://doi.org/10.3354/ame01306

Moisan TA, Mitchell BG (2018) Modeling net growth of *Phaeocystis antarctica* based on physiological and optical responses to light and temperature co-limitation. Front Mar Sci 4:365. https://doi.org/10.3389/fmars.2017.00437

Murata N, Takahashi S, Nishiyama Y, Allakhverdiev SI (2007) Photoinhibition of photosystem II under environmental stress. Biochim Biophys Acta 1767:414–421. https://doi.org/10.1016/j.bbabio.2006.11.019

Palmisano AC, Beeler SooHoo J, Sullivan CW (1987) Effects of four environmental variables on photosynthesis-irradiance relationships in Antarctic sea-ice microalgae. Mar Biol 94:299–306. https://doi.org/10.1007/BF00392944

Pankowski A, McMinn A (2009) Iron availability regulates growth, photosynthesis, and production of ferredoxin and flavodoxin in Antarctic sea ice diatoms. Aquat Biol 4:273–288. https://doi.org/10.3354/ab00116

Petrou K, Ralph PJ (2011) Photosynthesis and net primary productivity in three Antarctic diatoms: possible significance for their distribution in the Antarctic marine ecosystem. Mar Ecol Prog Ser 437:27–40. https://doi.org/10.3354/meps09291

Petrou K, Trimborn S, Rost B, Ralph PJ, Hassler CS (2014) The impact of iron limitation on the physiology of the Antarctic diatom *Chaetoceros simplex*. Mar Biol 161:925–937. https://doi.org/10.1007/s00227-014-2392-z

Quay PD, Peacock C, Björkman K, Karl DM (2010) Measuring primary production rates in the ocean: enigmatic results between incubation and non-incubation methods at station ALOHA. Glob Biogeochem Cycles. https://doi.org/10.1029/2009GB003665

Raven JA (2013) Iron acquisition and allocation in stramenopile algae. J Exp Bot 64:2119–2127. https://doi.org/10.1093/jxb/ert121

Regaudie-de-Gioux A, Duarte CM (2012) Temperature dependence of planktonic metabolism in the ocean. Glob Biogeochem Cycles. https://doi.org/10.1029/2010GB003907

Sarthou G, Timmermans KR, Blain S, Tréguer P (2005) Growth physiology and fate of diatoms in the ocean: a review. J Sea Res 53:25–42. https://doi.org/10.1016/j.seares.2004.01.007

Serret P, Robinson C, Aranguren-Gassis M, García-Martín EE, Gist N, Kitidis V, Lozano J, Stephens J, Harris C, Thomas R (2015) Both respiration and photosynthesis determine the scaling of plankton metabolism in the oligotrophic ocean. Nat Commun 6:6961. https://doi.org/10.1038/ncomms7961

Smetacek V, Klaas C, Strass VH, Assmy P, Montresor M, Cisewski B, Savoye N, Webb A, d'Ovidio F, Arrieta JM, Bathmann U, Bellerby R, Berg GM, Croot P, Gonzalez S, Henjes J, Herndl GJ, Hoffmann LJ, Leach H, Losch M, Mills MM, Neill C, Peeken I, Röttgers R, Sachs O, Sauter E, Schmidt MM, Schwarz J, Terbrüggen A, Wolf-Gladrow D (2012) Deep carbon export from a Southern Ocean iron-fertilized diatom bloom. Nature 487:313–319. https://doi.org/10.1038/nature11229

Stefels J, van Leeuwe MA (1998) Effects of iron and light stress on the biochemical composition of Antarctic *Phaeocystis* sp. (Prymnesiophyceae). I. Intracellular DMSP concentrations. J Phycol 34:486–495. https://doi.org/10.1046/j.1529-8817.1998.340486.x

Strzepek RF, Harrison PJ (2004) Photosynthetic architecture differs in coastal and oceanic diatoms. Nature 431:689–692. https://doi.org/10.1038/nature02954

Strzepek RF, Hunter KA, Frew RD, Harrison PJ, Boyd PW (2012) Iron-light interactions differ in Southern Ocean phytoplankton. Limnol Oceanogr 57:1182–1200. https://doi.org/10.4319/lo.2012.57.4.1182

Suggett DJ, MacIntyre HL, Geider RJ (2004) Evaluation of biophysical and optical determinations of light absorption by photosystem II in phytoplankton. Limnol Oceanogr Methods 2:316–332. https://doi.org/10.4319/lom.2004.2.316

Suggett DJ, Moore CM, Hickman AE, Geider RJ (2009) Interpretation of fast repetition rate (FRR) fluorescence: signatures of phytoplankton community structure versus physiological state. Mar Ecol Prog Ser 376:1–19. https://doi.org/10.3354/meps07830

Takao S, Hirawake T, Wright SW, Suzuki K (2012) Variations of net primary productivity and phytoplankton community composition in the Indian sector of the Southern Ocean as estimated from ocean color remote sensing data. Biogeosciences 9:3875–3890. https://doi.org/10.5194/bg-9-3875-2012

Thomas DN, Baumann ME, Gleitz M (1992) Efficiency of carbon assimilation and photoacclimation in a small unicellular *Chaetoceros* species from the Weddell Sea (Antarctica): influence of temperature and irradiance. J Exp Mar Biol Ecol 157:195–209. https://doi.org/10.1016/0022-0981(92)90162-4

Tilzer MM, Dubinsky Z (1987) Effects of temperature and day length on the mass balance of Antarctic phytoplankton. Polar Biol 7:35–42. https://doi.org/10.1007/BF00286822

Timmermans KR, Davey MS, van der Wagt B, Snoek J, Geider RJ, Veldhuis MJ, Gerringa LJ, de Baar HJ (2001) Co-limitation by iron and light of *Chaetoceros brevis*, *C. dichaeta* and *C. calcitrans* (Bacillariophyceae). Mar Ecol Prog Ser 217:287–297. https://doi.org/10.3354/meps217287

Tortell PD, Payne CD, Li Y, Trimborn S, Rost B, Smith WO, Riesselman C, Dunbar RB, Sedwick P, DiTullio GR (2008) CO_2 sensitivity of Southern Ocean phytoplankton. Geophys Res Lett 35:15587. https://doi.org/10.1029/2007GL032583

Tracewell CA, Vrettos JS, Bautista JA, Frank HA, Brudvig GW (2001) Carotenoid photooxidation in photosystem II. Arch Biochem Biophys 385:61–69. https://doi.org/10.1006/abbi.2000.2150

Tréguer P, Bowler C, Moriceau B, Dutkiewicz S, Gehlen M, Aumont O, Bittner L, Dugdale R, Finkel Z, Iudicone D, Jahn O, Guidi L, Lasbleiz M, Leblanc K, Levy M, Pondaven P (2018) Influence of diatom diversity on the ocean biological carbon pump. Nat Geosci 11:27–37. https://doi.org/10.1038/s41561-017-0028-x

Trimborn S, Thoms S, Petrou K, Kranz SA, Rost B (2014) Photophysiological responses of Southern Ocean phytoplankton to changes in CO_2 concentrations: short-term versus acclimation effects. J Exp Mar Biol Ecol 451:44–54. https://doi.org/10.1016/j.jembe.2013.11.001

Trimborn S, Hoppe CJ, Taylor BB, Bracher A, Hassler C (2015) Physiological characteristics of open ocean and coastal phytoplankton communities of Western Antarctic Peninsula and Drake Passage waters. Deep Sea Res I 98:115–124. https://doi.org/10.1016/j.dsr.2014.12.010

Trimborn S, Brenneis T, Hoppe CJ, Laglera LM, Norman L, Santos-Echeandía J, Völkner C, Wolf-Gladrow D, Hassler CS (2017) Iron sources alter the response of Southern Ocean phytoplankton to ocean acidification. Mar Ecol Prog Ser 578:35–50. https://doi.org/10.3354/meps12250

Trimborn S, Thoms S, Bischof K, Beszteri S (2019) Susceptibility of two southern ocean phytoplankton key species to iron limitation and high light. Front Mar Sci 6:1248. https://doi.org/10.3389/fmars.2019.00167

Twining BS, Baines SB (2013) The trace metal composition of marine phytoplankton. Ann Rev Mar Sci 5:191–215. https://doi.org/10.1146/annurev-marine-121211-172322

van de Poll WH, Janknegt PJ, van Leeuwe MA, Visser RJW, Buma AGJ (2009) Excessive irradiance and antioxidant responses of

an Antarctic marine diatom exposed to iron limitation and to dynamic irradiance. J Photochem Photobiol B 94:32–37. https://doi.org/10.1016/j.jphotobiol.2008.09.003

van de Poll WH, Lagunas M, de Vries T, Visser RJ, Buma AG (2011) Non-photochemical quenching of chlorophyll fluorescence and xanthophyll cycle responses after excess PAR and UVR in *Chaetoceros brevis*, *Phaeocystis antarctica* and coastal Antarctic phytoplankton. Mar Ecol Prog Ser 426:119–131. https://doi.org/10.3354/meps09000

van Oijen T, van Leeuwe MA, Gieskes WWC, de Baar HJW (2004) Effects of iron limitation on photosynthesis and carbohydrate metabolism in the Antarctic diatom *Chaetoceros brevis* (Bacillariophyceae). Eur J Phycol 39:161–171. https://doi.org/10.1080/0967026042000202127

Verity PG (1982) Effects of temperature, irradiance, and daylength on the marine diatom *Leptocylindrus danicus* Cleve. III. Dark respiration. J Exp Mar Biol Ecol 60:197–207. https://doi.org/10.1016/0022-0981(82)90159-9

Vona V, Di Martino RV, Lobosco O, Carfagna S, Esposito S, Rigano C (2004) Temperature responses of growth, photosynthesis, respiration and NADH: nitrate reductase in cryophilic and mesophilic algae. New Phytol 163:325–331. https://doi.org/10.1111/j.1469-8137.2004.01098.x

Wilhelm C, Wild A (1984) The variability of the photosynthetic unit in *Chlorella* II. the effect of light intensity and cell development on photosynthesis, P-700 and cytochrome f in homocontinuous and synchronous cultures of *Chlorella*. J Plant Physiol 115:125–135. https://doi.org/10.1016/S0176-1617(84)80059-0

Wright SW, Jeffrey SW, Mantoura RF, Llewellyn CA, Bjornland T, Repeta D, Welschmeyer N (1991) Improved HPLC method for the analysis of chlorophylls and carotenoids from marine phytoplankton. Mar Ecol Prog Ser 77:183–196. https://doi.org/10.3354/meps077183

Yoon J-E, Yoo K-C, Macdonald AM, Yoon H-I, Park K-T, Yang EJ, Kim H-C, Lee JI, Lee MK, Jung J, Park J, Lee J, Kim S, Kim S-S, Kim K, Kim I-N (2018) Reviews and syntheses: ocean iron fertilization experiments—past, present, and future looking to a future Korean Iron Fertilization Experiment in the Southern Ocean (KIFES) project. Biogeosciences 15:5847–5889. https://doi.org/10.5194/bg-15-5847-2018

Zhu Z, Xu K, Fu F, Spackeen JL, Bronk DA, Hutchins DA (2016) A comparative study of iron and temperature interactive effects on diatoms and *Phaeocystis antarctica* from the Ross Sea. Antarct Mar Ecol Prog Ser 550:39–51. https://doi.org/10.3354/meps11732